Extreme weather events in early Summer 2018 connected by a recurrent hemispheric wave pattern.

Kai Kornhuber[1,2], Scott Osprey[1,2], Dim Coumou[3,4], Stefan Petri[3],

Vladimir Petoukhov[3], Stefan Rahmstorf[3], Lesley Gray[1,2]

[1]Atmospheric, Oceanic and Planetary Physics, University of Oxford, Oxford, United Kingdom
[2]National Centre for Atmospheric Science, United Kingdom
[3]Earth System Analysis, Potsdam Institute for Climate Impact Research, Potsdam, Germany
[4]Institute for Environmental Studies, Vrije Universiteit Amsterdam, Amsterdam, Netherlands

Corresponding author: Kai Kornhuber (kai.kornhuber@physics.ox.ac.uk)

Key Points:

- We identify a recurrent Rossby-wave 7 teleconnection in Northern Hemisphere summer that exhibits a fixed phase position.
- It has been observed during summers that featured extreme heat-waves in Central US, Western Europe and the Caspian Sea region.
- This teleconnection was related to several regional weather extremes occurring near simultaneously across the mid-latitudes in June-July 2018.

Abstract

The summer of 2018 witnessed a number of extreme weather events such as heatwaves in North America, Western Europe and the Caspian Sea region and rainfall extremes in South-East Europe and Japan that occurred near-simultaneously. Here we show that these extremes were connected by an amplified hemisphere-wide wavenumber 7 circulation pattern. We show that this pattern constitutes a teleconnection in Northern Hemisphere summer associated with prolonged and above-normal temperatures in North America, Western Europe and the Caspian Sea region. This pattern was also observed during the European heatwaves of 2003, 2006, 2012 and 2015 among others. We show that the occurrence of this wave 7 pattern has increased over recent decades.

Plain Language Summary

During late June through to July 2018 a prolonged circumpolar circulation pattern linked weather extremes in North America, Western Europe, the Caspian Sea and Japan. We identified this pattern be a recurrent teleconnection pattern leading to heat extremes in specific regions, also observed during several other extreme summers.

1 Introduction

Boreal summer of 2018 saw several record breaking and persistent heat and rainfall extremes occurring simultaneously in the Northern Hemisphere (NH) mid-latitudes. In North America, Los Angeles and Montreal all-time high temperature records were set early in July leading to power outages and severe heat stress. In Western Europe, the UK experienced a record long drought and heat for 40 days lasting from mid-June to mid-July (*1*, *2*). In Glasgow and Belfast all-time record temperatures were measured on June 28 (32°C, 29.5°C) and the ongoing drought conditions triggered water restrictions. Meanwhile, in Georgia and Yerevan record temperatures above 40°C were measured (also see areas witnessing record breaking temperatures in Fig. S2b). Further, heavy rainfall over Greece, Romania, Ukraine and Bulgaria at the end of June led to severe flooding damage (*3*). Early July extreme rainfall over Japan caused landslides and flooding (*1*) killing at least 120 people (also see section: *Japanese Floods* and Fig. S1 in Supplementary Materials).

2 Materials and Methods

Linear regression of the time-series shown in Fig. 4 C, D of the manuscript was done using a least-square fitting algorithm. Significance was defined at the 95% confidence level.

The surface temperature composite anomaly field (Fig 4. A, B) was determined from weekly temperature anomaly fields based on grid-point-wise detrended daily surface

temperature fields from NCEP.NCAR. Significance was determined by comparing high amplitude events (>1.5σ) with the mean of all remaining weeks using a t-test and an adjusted p-value determined by false discovery rate testing (FDR)(*2*).

Spectral decomposition of weekly averaged meridional wind at 300mb and orography fields into their basic components and phases (Fig. 3, Fig. 4) was done using a fast fourier transformation applied on their mid-latitudinal average 37.5° N – 57.5° N (*3*).

Phase velocities shown in Fig. 2e were determined from by taking a fourth-order accurate numerical approximation of the transient derivative of its phase based on daily data following Coumou et al. 2014 (3). In a second step 15-day running mean values of these daily phase velocities are calculated.

3 Data

Daily wind and temperature data were taken from the archives of the European Center for Medium Range Weather Forecasts (ECMWF) and the National Oceanic and Atmospheric Administration (NOAA, NCEP-NCAR reanalysis (*1*)). In order to avoid spurious trends due to changes in measurement systems we limited the analysis to the satellite based period (1979 – 2018).

4 Results

Here we show that these devastating extreme weather events were linked by a hemispheric-scale circulation pattern, characterized by a strongly meandering wave-like jet-stream stretching across the entire hemisphere (between ~30-60°N in Fig. 1b). This wave-like structure created alternating patterns of anomalously warm and cold conditions, setting the stage for hot-dry extremes and persistent rain throughout the mid-latitudes (Fig. 1a, also see Fig. S2). The circulation regime of summer 2018 was remarkable, not only in terms of the amplitude and regularity of the wave-pattern but also due to its persistence, lasting for about 2-3 weeks from late-June to early-July.

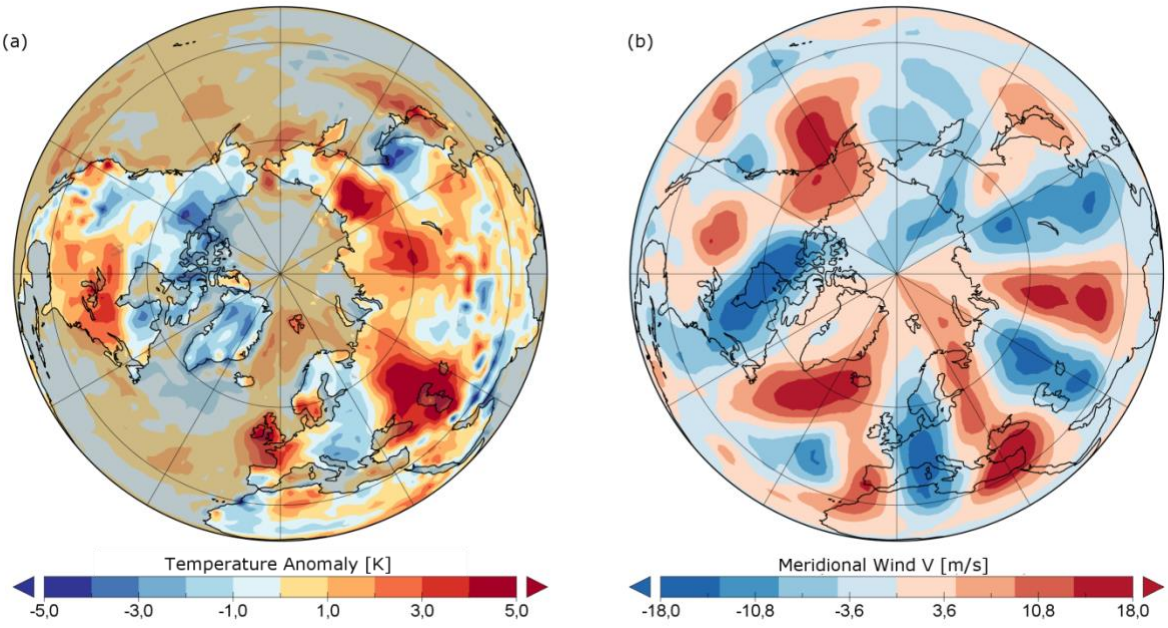

Figure 1. Northern Hemisphere temperature anomalies and stationary Rossby wave pattern in early July. (a) Surface temperature Anomalies (from 1981-2010 climatology; 15-day mean, centered on July 1st 2018). Oceans are masked in transparent grey. (**b)** As (A) but for meridional wind V (m s^{-1}) in the upper troposphere (250 mb).

This strongly meandering circulation regime created the necessary background conditions for many simultaneous weather extremes. Figure 2b shows the onset and persistence of the wave pattern as a Hovmöller plot (longitude vs. time) of the meridional winds averaged over the mid-latitudes (37.5°N-57.5°N, with the timing and longitudinal location of notable extreme weather events superimposed. Starting at the end of June, a quasi-stationary wavenumber 7 (wave 7 from hereon) circulation pattern evolves (Fig. S3a,b), with large amplitude (Fig. 2b, c, Fig.S3c), near-stationary phase position (Fig. 2d) and near-zero phase speed (Fig. 2e). The amplitude starts to increase from mid-June, exceeding the 1.5 standard deviation threshold by the end of June (Fig. 2c) and persists at that high level until early July. In concert with the rising amplitude, the wave phase-shifts into a preferred position where it persists (indicated by the dashed red lines in Fig. 2D, also see Fig. S4). The absolute phase speed of wave 7 slows down at the moment when the preferred phase position is reached. Coinciding with the peak of the stationary pattern from end of June to early July several heat and rainfall extremes occur in the mid-latitudes (Fig. 2b, Fig. S2b).

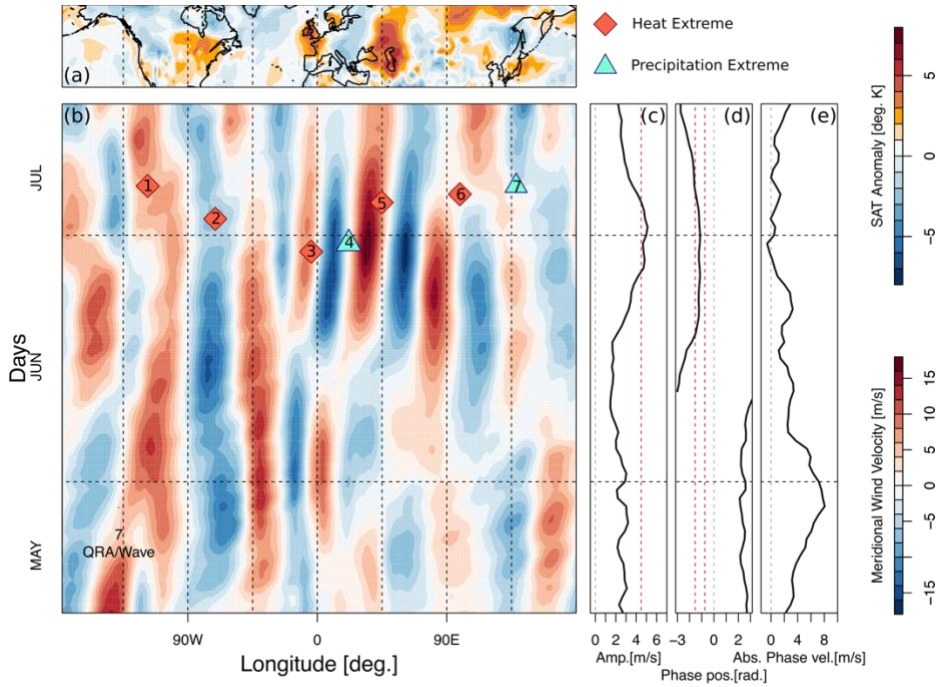

Figure 2. Time evolution of persistent wave 7 circulation pattern. (a) NH surface air temperatures (15-day mean centered on July 1st 2018). **(b)** Hovmöller (longitude-time) time evolution of the mid. latitude (averaged over 37.5°N – 57.5°N) meridional winds. A stationary wave 7 pattern evolves in mid. June. The location and timing of extreme events are marked as orange diamond (heat extreme) and blue triangle (precipitation extreme); from left to right: (1) Los Angeles, (2) Montreal, (3) Belfast, (4) Sofia, (5) Tiflis, (6) Siberia, (7) Hiroshima. **(c)** Amplitude of wave 7 (m s^{-1}). The amplitude increases and exceeds 1.5 std (red dashed line) at end of June shortly before heat records are broken across the mid-latitudes (also see Fig. S2b). **(d)** Phase of wave 7 (radians). The phase becomes locked within its preferred position (marked by red dashed lines) by mid-June. **(e)** Phase speed of wave 7 (m s^{-1}). The phase speed slows down in concert with the increasing amplitude and the phase locking of wavenumber 7.

Here we show that wave 7 is of particular importance, as it shows some unique behavior in that it tends to get locked in a specific preferred phase position as the amplitude increases and remain there for an extended period (*4*) (also see Fig. S4), constituting circumglobal teleconnection pattern in NH Summer. This is consistent with the work from Branstator et al. (*5*) who showed that zonally elongated zonal winds (see Fig. S9) can act as waveguides for planetary waves leading to co-variability in far-away regions (*6*).

The hemispheric circulation exhibits spatially confined troughs and ridges which then persist over specific regions (Fig.3b) (*4*, *7*). A characteristic circumglobal pattern of alternating temperature anomalies thus arises across the mid-latitudinal belt with significantly elevated surface temperatures over central North America, Western/Central Europe and the Caspian Sea region (Fig. 3a), just as observed in summer 2018 (Fig. 1a, Fig. 2a). Here, high amplitude wave 7 events were defined by weeks in JJA exceeding 1.5σ (the pattern however is independent on the exact choice of threshold; see Fig. S5). In the regions identified above, dynamic contributions from the wave 7 circumglobal teleconnection can then intensify the normal summer temperatures and lead to heat waves on weekly to monthly time scales.

In agreement, many of high amplitude wave 7 events coincide with heat extremes in Central North America and central Western Europe and the Caspian Sea region as suggested by the surface temperature anomaly map (Fig. 3a), among them the devastating heatwaves of 2003, 2006, 2012 and 2015 (*4*, *8*) (also see Fig. S6, Table S1).

Over recent decades the number of wave 7 *phase-locked* events (here defined as weeks with above average wave 7 amplitude within its preferred position, see Fig. S3) have increased significantly (0.95 confidence interval (Fig. 4b). Summers with more than one subsequent week of wave 7 phase-locked events did not occur prior to 1999, but since then have occurred at an increasing frequency (Table S1). This can be interpreted as an increase in persistence of such situations. In fact, the average number has doubled from about one to two weeks per year, while the number of years with more than two events per summer shows an almost eight-fold increase. Although the sign of the trend is independent of the applied amplitude threshold, the significance of the trend depends on the amplitude threshold, possibly due to the consequent reduction in ensemble size (Fig. 4b). The number of wave 7 events (weeks exceeding a specific wave amplitude threshold) show increasing but not significant trends independent of threshold applied (Fig. 4a). A significant trend for the amplitude of wave 7 in summer is only found when including data beyond the satellite measurement period (Fig. S7). In general, these trends should be treated cautiously as the period of satellite observations (1979 onwards) is relatively short and they might thus reflect multi-decadal oscillations in the earth system.

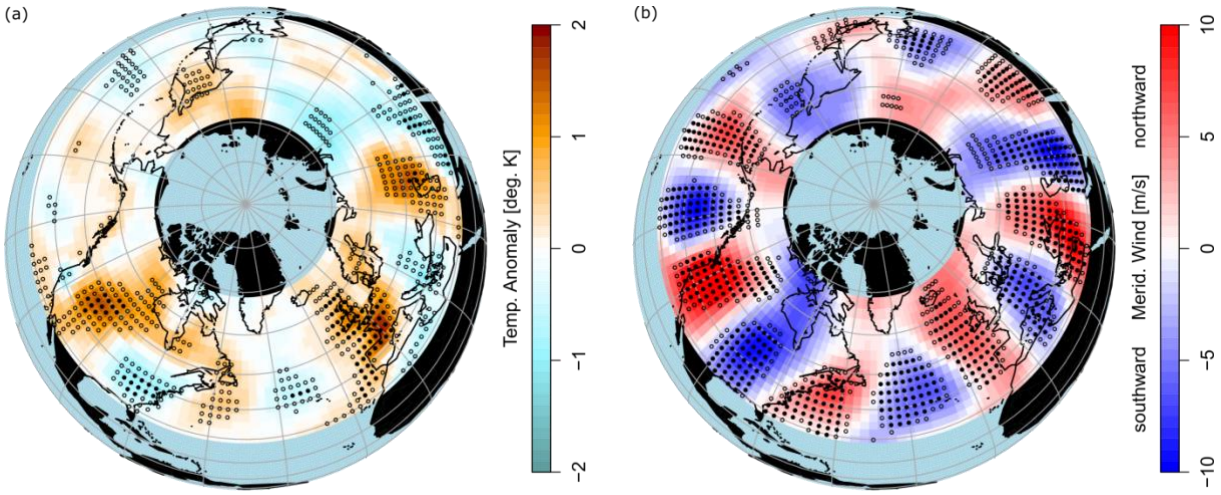

Figure 3. A recurrent circumglobal wave 7 teleconnection. (a) Composite plot of surface temperature anomalies over the NH mid-latitudes (30°N - 67.5°N) during weeks of high wave 7 amplitudes (>1.5σ, N: 40 weeks) in summer (JJA) over the NH mid-latitudes (30°N - 67.5°N) observed over the period 1979 - 2016. **(b)** Meridional wind speeds (northward: red; southward: blue) during those events. The filled stippling in (**a**) and (**b**) indicates grid-cells with significant deviations from JJA climatology using a significance test that accounts for the false discovery rate (FDR) associated with multiple testing (*9*), while the grid-points marked with hollow stippling indicate local significance.

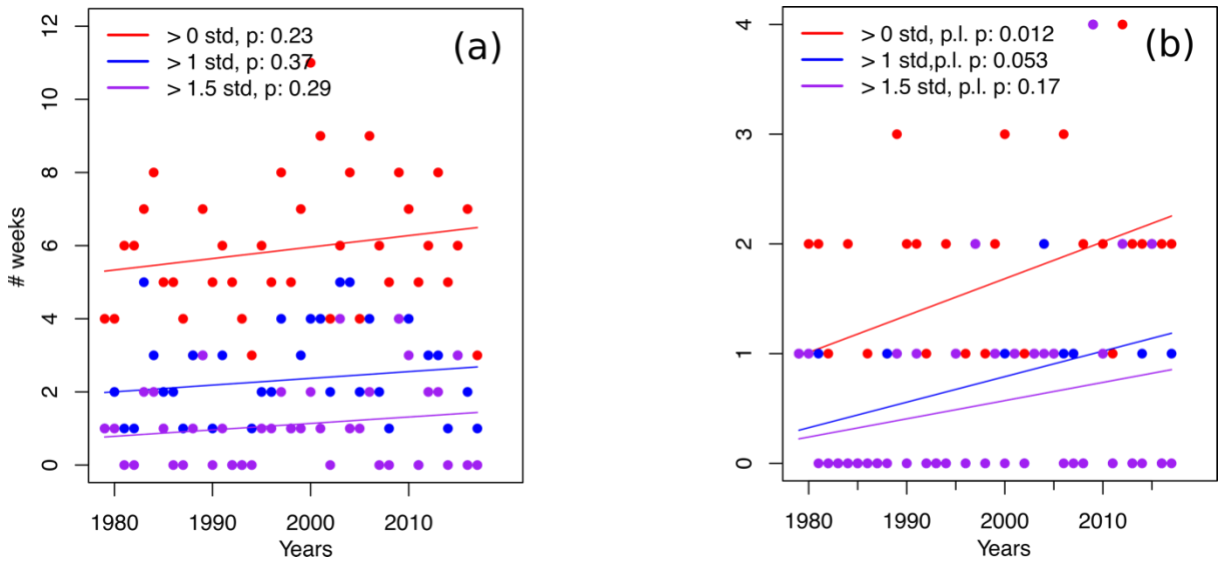

Figure 4. Recent trends in the occurrence of the wave 7 teleconnection. **(a)** Number of weeks per summer season (JJA) with wave 7 amplitude above average (>0σ)**,** 1σ and

1.5σ irrespective of phase position. (**b)** Number of weeks per summer season (JJA) where wave seven is in its preferred phase position (see Fig. S3) and the amplitude of wave 7 is above average (>0σ), >1 σ and >1.5σ.

5 Conclusions

It is important to note that extreme weather events such as the heatwaves observed in Summer 2018 are the product of several factors acting together. For example it has been shown that the Extreme heatwaves in Europe 2003 and Russia 2010 were preceded by very low soil moisture content due to an anomalous dry spring season (*10–12*) and there is good reasons to believe that the anomalously dry April-May conditions in many parts of the NH contributed to a large degree to the magnitude and persistence of the observed heatwaves by known soil moisture feedbacks. In general, record breaking heat and rainfall extremes are the expected outcome of a warming mean climate due to increasing greenhouse gas (GHG) emissions (*13*, *14*). GHG warming leads to more intense events heat and an enhanced water holding capacity of the air which fuels heavy rainfall. The timing, duration and location of a specific extreme weather event, however is largely controlled by the large scale circulation, especially in the mid-latitudes (*15*). While the direct response to thermodynamic drivers of weather extremes are generally well understood, large uncertainty remains when it comes to the indirect response via the changes in dynamical circulation drivers under a warmer climate (*15–19*). Changes in the dynamical circulation have been proposed to explain the increase in persistence and magnitude of recent summer extremes, that have exceeded what would be expected from simple thermodynamic arguments (*19*, *20*), particularly in the case of Western and Central Europe as well as the Southern Central US being repeatedly struck by devastating heatwaves (*12*, *21–24*). Summer storm tracks have been weakening over recent decades (*25*) which likely influences planetary wave behavior. In boreal summer Rossby waves have indeed been increasing recently in agreement with our results (*26*). Others however have shown that upward trends over a relatively short period are not statistically significant (*27*) and traditional blocking indices show no changes in summer (*28*). The regions for which an increase in the persistence of regional weather regimes was identified, however, (Northern US, Europe and Western Asia) match those related to the wave 7 teleconnection pattern (*29*). Planetary wave resonance has been discussed as a potential mechanism to generate high amplitude synoptic wave patterns in boreal summer (*4*, *8*, *30*) and required conditions were present in June July as well (also see discussion in SI). Recent trends in the zonal temperature profile due to anthropogenic climate change have been suggested to favour resonance conditions (*31*). This temperature profile bears imprints of enhanced land warming and high latitude warming and is associated with the formation of double-jets in the zonal mean zonal wind (*8*, *31*). In the given case a double

jet pattern was visible over the Eurasian continent (Fig. S9), which might be the reason that planetary wave patterns were specifically amplified and persistent.

In summary, we have shown that the summer 2018 featured a series of near simultaneous extreme weather events that coincided in time and space with a circumglobal teleconnection constituted by an amplified Rossby wave of wavenumber 7 in the mid-latitude jet stream. These extremes include the heat-records of June/July broken in North America, Western Europe and Caspian Sea region, as well as the extreme and devastating rainfall events in South-East Europe and Japan. Tropical ENSO variability in 2018 was in a neutral state and thus unlikely to be an important factor behind the extreme weather events in the NH. This recurrent circulation pattern conducive for heat waves acts in addition to the thermodynamically driven increase in heat, creating possibilities for very-extreme heat waves, specifically in the identified regions: Western Europe, North America and Caspian Sea region. We show that this circumglobal teleconnection pattern has increased in frequency and persistence in recent years. Given the high impacts of these extremes in terms of mortality, morbidity and agricultural losses, this presents major risks for society and global food production in particular, since the main breadbasket regions are located in the mid-latitudes. Further research is required to fully understand the combination of factors that trigger these observed wave events, and what determines their preferred phase position, so that predictability of future extreme events can be improved.

References:

1. NOAA, "State of the Climate: Global Climate Report for July 2018" (2018), (available at https://www.ncdc.noaa.gov/sotc/global/201807).

2. NOAA, "State of the Climate: Global Climate Report for June 2018" (2018), (available at https://www.ncdc.noaa.gov/sotc/global/201806).

3. International Federation of Red Cross and Red Crescent Societies, "Information Bulletin no. 1 Flash floods in Europe" (2018).

4. K. Kornhuber *et al.*, Summertime Planetary Wave-Resonance in the Northern and Southern Hemisphere. *J. Clim.* **30**, 6133–6150 (2017).

5. G. Branstator, Circumglobal Teleconnections, the Jet Stream Waveguide, and the North Atlantic Oscillation. *J. Clim.* **15**, 1893–1910 (2002).

6. G. Branstator, H. Teng, Tropospheric Waveguide Teleconnections and Their Seasonality. *J. Atmos. Sci.* **74**, 1513–1532 (2017).

7. J. Zhang, J. Yuanchun, C. Haishan, W. Zhiwei, Double-mode adjustment of Tibetan Plateau heating to the summer circumglobal teleconnection in the Northern Hemisphere.

Int. J. Climatol. (2017), doi:10.1002/joc.5201.

8. K. Kornhuber, V. Petoukhov, S. Petri, S. Rahmstorf, D. Coumou, Evidence for wave resonance as a key mechanism for generating high-amplitude quasi-stationary waves in boreal summer. *Clim. Dyn.* **49**, 1961–1979 (2017).

9. D. Wilks, " the Stippling Shows Statistically Significant Grid Points ." *Bull. Am. Meteorol. Soc.* **97**, 2263–2274 (2016).

10. E. M. Fischer, S. I. Seneviratne, D. Lüthi, C. Schär, Contribution of land-atmosphere coupling to recent European summer heat waves. *Geophys. Res. Lett.* **34**, L06707 (2007).

11. D. G. Miralles, A. J. Teuling, C. C. van Heerwaarden, J. Vilà-Guerau de Arellano, Mega-heatwave temperatures due to combined soil desiccation and atmospheric heat accumulation. *Nat. Geosci.* **7**, 345–349 (2014).

12. E. Black, M. Blackburn, G. Harrison, B. Hoskins, J. Methven, Factors contributing to the summer 2003 European heatwave. *Weather*. **59**, 217–223 (2004).

13. J. Lehmann, D. Coumou, K. Frieler, Increased record-breaking precipitation events under global warming. *Clim. Change*. **132**, 501–515 (2015).

14. S. Rahmstorf, D. Coumou, Increase of extreme events in a warming world. *Proc. Natl. Acad. Sci. U. S. A.* **108**, 17905–9 (2011).

15. T. G. Shepherd, Atmospheric circulation as a source of uncertainty in climate change projections. *Nat. Geosci.* **7**, 703–708 (2014).

16. J. Cohen *et al.*, Recent Arctic amplification and extreme mid-latitude weather. *Nat. Geosci.* **7**, 627–637 (2014).

17. E. A. Barnes, J. A. Screen, The impact of Arctic warming on the midlatitude jet-stream: Can it? Has it? Will it? *Wiley Interdiscip. Rev. Clim. Chang.* (2015) (available at http://doi.wiley.com/10.1002/wcc.337).

18. B. Hoskins, T. Woollings, Persistent Extratropical Regimes and Climate Extremes. *Curr. Clim. Chang. Reports*. **1**, 115–124 (2015).

19. R. M. Horton, J. S. Mankin, C. Lesk, E. Coffel, C. Raymond, A Review of Recent Advances in Research on Extreme Heat Events. *Curr. Clim. Chang. Reports*. **2**, 242–259 (2016).

20. J. Luterbacher *et al.*, European Seasonal and Annual Temperature Variability, Trends, and Extremes Since 1500. *Science (80-.).* **303**, 1499–1503 (2004).

21. A. Hoy, S. Hänsel, P. Skalak, Z. Ustrnul, O. Bochníček, The extreme European summer of 2015 in a long-term perspective. *Int. J. Climatol.*, 1–20 (2016).

22. M. Rebetez, O. Dupont, M. Giroud, An analysis of the July 2006 heatwave extent in Europe compared to the record year of 2003. *Theor. Appl. Climatol.* **95**, 1–7 (2009).

23. M. Hoerling, J. K. Eischeid, X. Quan, T. Xu, Explaining the record US warmth of 2006. *Geophys. Res. Lett.* **34**, 1–4 (2007).

24. N. S. Diffenbaugh, M. Scherer, Likelihood of July 2012 U.S. temperatures in preindustrial and current forcing regimes. *Bull. Am. Meteorol. Soc.*, 6–9 (2013).

25. D. Coumou, J. Lehmann, J. Beckmann, The weakening summer circulation in the Northern Hemisphere mid-latitudes. *Science (80-.).* **348**, 324–327 (2015).

26. S.-Y. Wang, R. E. Davies, R. R. Gillies, Identification of extreme precipitation threat across midlatitude regions based on short-wave circulations. *J. Geophys. Res. Atmos.* **118**, 11059–11074 (2013).

27. J. A. Screen, I. Simmonds, Exploring links between Arctic ampli fi cation and mid-latitude weather. **40**, 959–964 (2013).

28. T. Woollings *et al.*, Blocking and its Response to Climate Change. *Curr. Clim. Chang. Reports*, 1–14 (2018).

29. D. E. Horton *et al.*, Contribution of changes in atmospheric circulation patterns to extreme temperature trends. *Nature*. **522**, 465–469 (2015).

30. V. Petoukhov, S. Rahmstorf, S. Petri, H. J. Schellnhuber, Quasiresonant amplification of planetary waves and recent Northern Hemisphere weather extremes. *Proc. Natl. Acad. Sci.* **110**, 5336–41 (2013).

31. M. E. Mann *et al.*, Influence of Anthropogenic Climate Change on Planetary Wave Resonance and Extreme Weather Events. *Sci. Rep.* **7**, 45242 (2017).

Acknowledgements:

We thank the European Centre for Medium Range Weather Forecasts (ECMWF) for access to their Operational Analysis data and the federal state of Brandenburg is acknowledged for supporting the used high-performance computing resources. **Funding**: This work was supported by the UK Natural Environment Research Council (NERC) National Centre for Atmospheric Science (NCAS) and NERC grants NE/P006779/1 and NE/N018001/1 (K.K., L.G. and S.O.) and by the German Federal Ministry of Education and Research (BMBF) and by the Netherlands Organisation for Scientific Research (NWO) (D.C). **Author contributions**: K.K., S.O., D.C., L.G. conceptualised the paper. K.K. undertook the analysis. All authors contributed to the writing of the paper. **Competing Interests**: The authors declare no competing interests. **Data and materials availability**: The data used in this study can be obtained from the ECMWF and NCEP-NCAR websites or via the UK Centre for Environmental Data Analysis (CEDA)

Supporting Information for

Extreme weather events in early summer 2018 connected by a recurrent hemispheric wave pattern

Kai Kornhuber [1,2*], Scott Osprey [1,2], Dim Coumou [3,4], Stefan Petri [3],

Vladimir Petoukhov [3], Stefan Rahmstorf [3], Lesley Gray [1,2]

[1]Atmospheric, Oceanic and Planetary Physics, University of Oxford, Oxford, United Kingdom

[2]National Centre for Atmospheric Science, United Kingdom

[3]Earth System Analysis, Potsdam Institute for Climate Impact Research, Potsdam, Germany

[4]Institute for Environmental Studies, Vrije Universiteit Amsterdam, Amsterdam, Netherlands

*Corresponding author: kai.kornhuber@physics.ox.ac.uk

Contents of this file

Text S1. Japanese Floods early July 2018.

From late June through to early July the slow-moving circulation identified over Eurasia coincided with large high-pressure systems north and east of Japan (Fig. S1). This confined a north-east flow of warm moist air over Japan from lower latitudes. At the same time a seasonally stalled Meiyu weather front stretched across Japan causing persistent rainfall in the south-west Okinawa prefecture . These persistent rains were further exacerbated by the passage of ex-tropical storm Prapiroon over the affected areas, causing major flooding. A meandering atmospheric river of high moisture laden air is clearly evident in Fig. S1a at the time of this flooding event, which is clearly influenced by the background slow moving circulation patterns seen in Fig. S1b.

Text S2. Quasi-resonant amplification during June-July 2018.

Quasi-resonant amplification (QRA) was proposed as a dynamical mechanism that could lead to the high-amplitude planetary waves of synoptic scale wavenumbers 6-8 (4–6). The QRA mechanism as derived by Petoukhov et al. (4) assumes that 'a synoptic-scale free wave trapped in a midlatitude waveguide can resonate with the slow-moving forced wave and thereby increase its amplitude through a quasi-resonant amplification' (6). This framework thus differs from the concept of 'resonance' described in Held 1983(12) as waves are not assumed to encircle the longitudinal belt to interact with the "tails" of themselves (also see our reply to comment 1). The theory behind this mechanism is based on linear theory, and assumes a zonally symmetric background flow on which perturbations develop (7, 13) but it only considers zonally elongated waves (in contrast to e.g. Hoskins & Karoly (7) who discuss meridionally propagating waves). It describes similar phenomena as Branstator et al. (8, 9) who showed that circumglobal wave patterns can evolve when a waveguide is provided in zonal direction by a mid-latitudinal jet. A zonal waveguide effectively traps those waves in the mid-latitudes, preventing their dissipation in the meridional direction, which is the first precondition for QRA.

We tested the resonance conditions (Table S2) for the 2018 summer following the methodology of (2) (see Table S2 for details). Figure S8 provides evidence that the persistent wave 7 circulation pattern is consistent with the resonance of atmospheric waves trapped in a mid-latitude waveguide. It shows the time evolution of the prime quantities associated with wave resonance: The zonally averaged zonal wind U as a measure for the background flow (Fig. S8a),

the squared meridional wavenumber (l2) that determines waveguide formation (Fig.S8b) which is critical for resonance detection (Fig. S8c). A 'double jet' in the zonal mean jet evolves in early June (i.e. two peaks in U at ~45N and 75N). This configuration in the zonal mean zonal wind is characterized by a narrow subtropical jet with sharp edges which is known to favor waveguides (14). Figure S9 shows a 15-day average of the zonal wind field centered around the 1st July 2018. The zonal winds form a near circumglobal jet, which splits into a double jet configuration at 15W over Eurasia. A waveguide forms for wave 7 as indicated by the two turning points in l2 (dotted black lines in Fig. S8b). The detection scheme also indicates sufficient orographic / thermal forcing and therefore resonance is detected from mid-June onwards (Fig. 2b, S8c). As expected from resonance theory (4), a few days later the phase speed of wave 7 slows down and the amplitude increases to a level above 1.5 standard deviations (Fig. 2d, e).

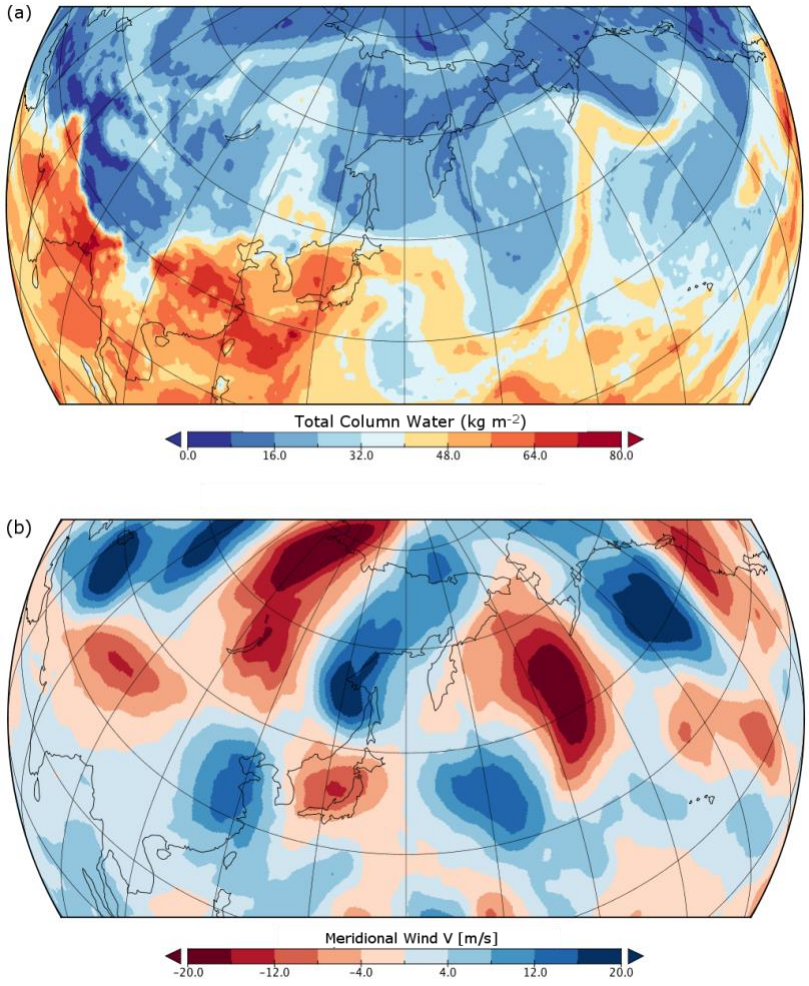

Figure S1. The role of the large-scale circulation in the Japanese Floods 2018. (A) Total column water measured 4th of July over the East Asian Pacific Sector (B) Meridional windspeeds centered on 4th July (7-day running average)**.**

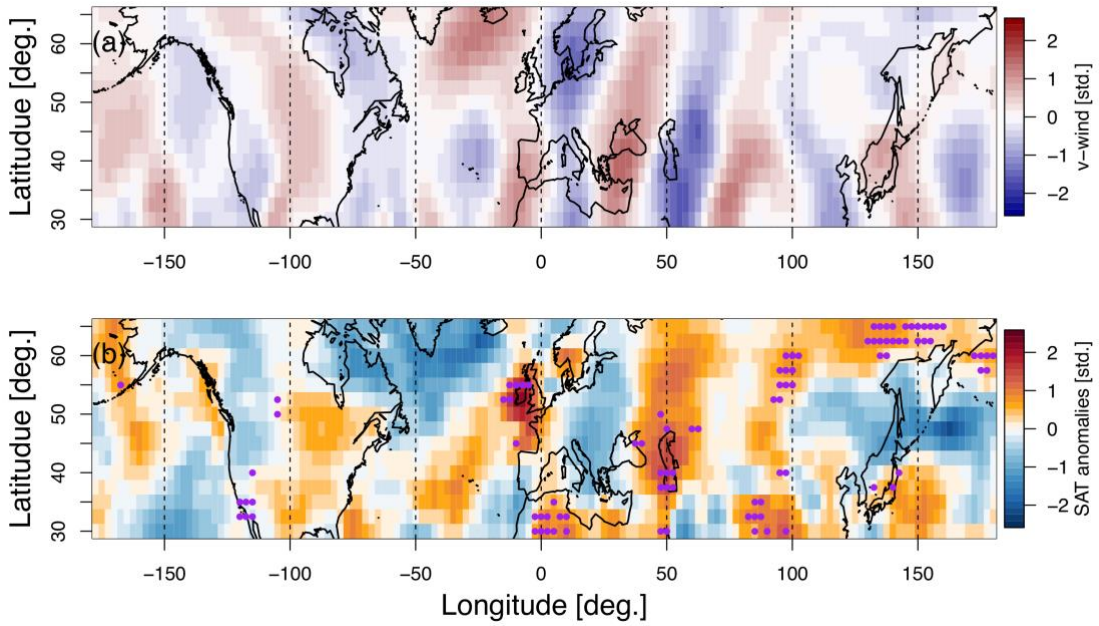

Figure S2. Meridional winds and surface temperature anomalies in units of standard deviation. (a) 15-day average of daily anomalies in units of standard deviation centered around the 1st of July 2018. The meridional winds are arranged in form of a circumglobal wave pattern specifically in the mid-latitudinal belt (30N- 55N). (b) Same as in (a) but for linearly detrended temperature anomalies. Temperature anomalies occur in line with the position of ridges and troughs of the circumglobal wave pattern depicted in (b), reaching values of above 2 std. in Europe and above 1 std. in Central US, the Caspian Sea region, Northern China, Siberia and Japan. Grid-points that exhibit daily record temperatures within the 15-day window around the 1st of July are marked by purple dots. Those grid-points agree well with the regions marked in Fig.2 in the main manuscript.

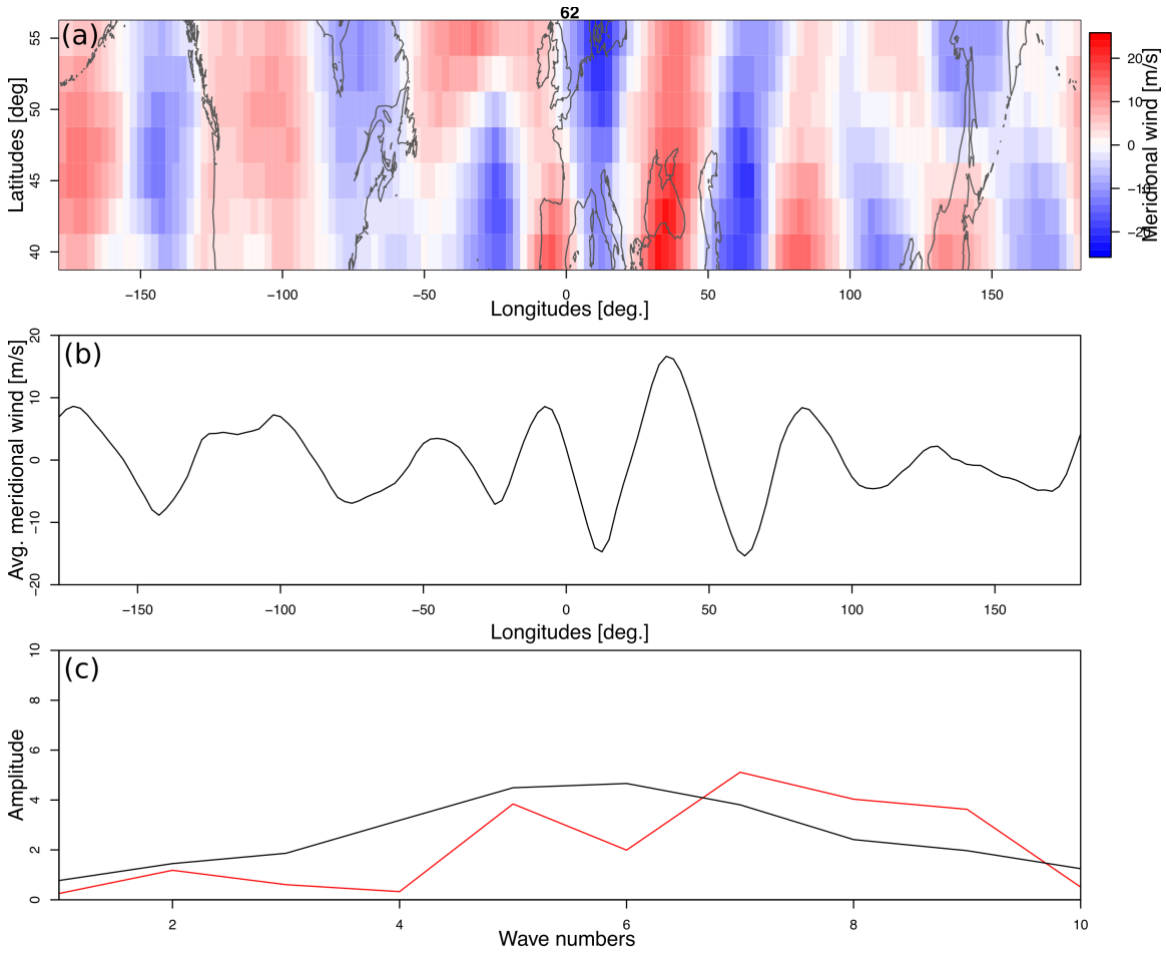

Figure S3. A circumglobal wave pattern during Jun-July 2018. (a) Meridional winds (15 day mean centered around the 1. Of July). (B) the meridional averaged meridional winds in the mid. latitudinal belt (37.5N-57.5N). (c) Rossby wave amplitudes of wavenumbers 1-10 determined by applying a Fast-Fourier-Transformation on the data shown in (b).

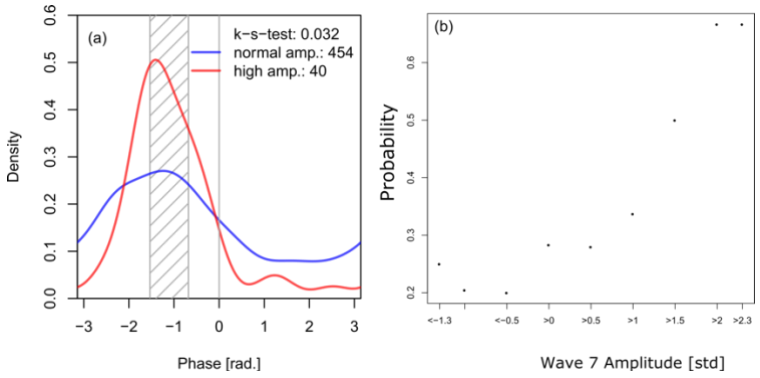

Figure S4. Evidence for a circumglobal wave 7 Teleconnection. (a) Probability density distributions during summer (JJA), comparing weeks of high amplitude (> 1.5σ, red) and normal amplitude (< 1.5σ, blue) of wave 7 (b) Probability of a week in summer (JJA) to exhibit phase of wavenumber 7 within the phase locked region as defined by the 25th -75th percentile of the high amplitude wave 7 (> 1.5σ). The probability increases with amplitude of wave 7.

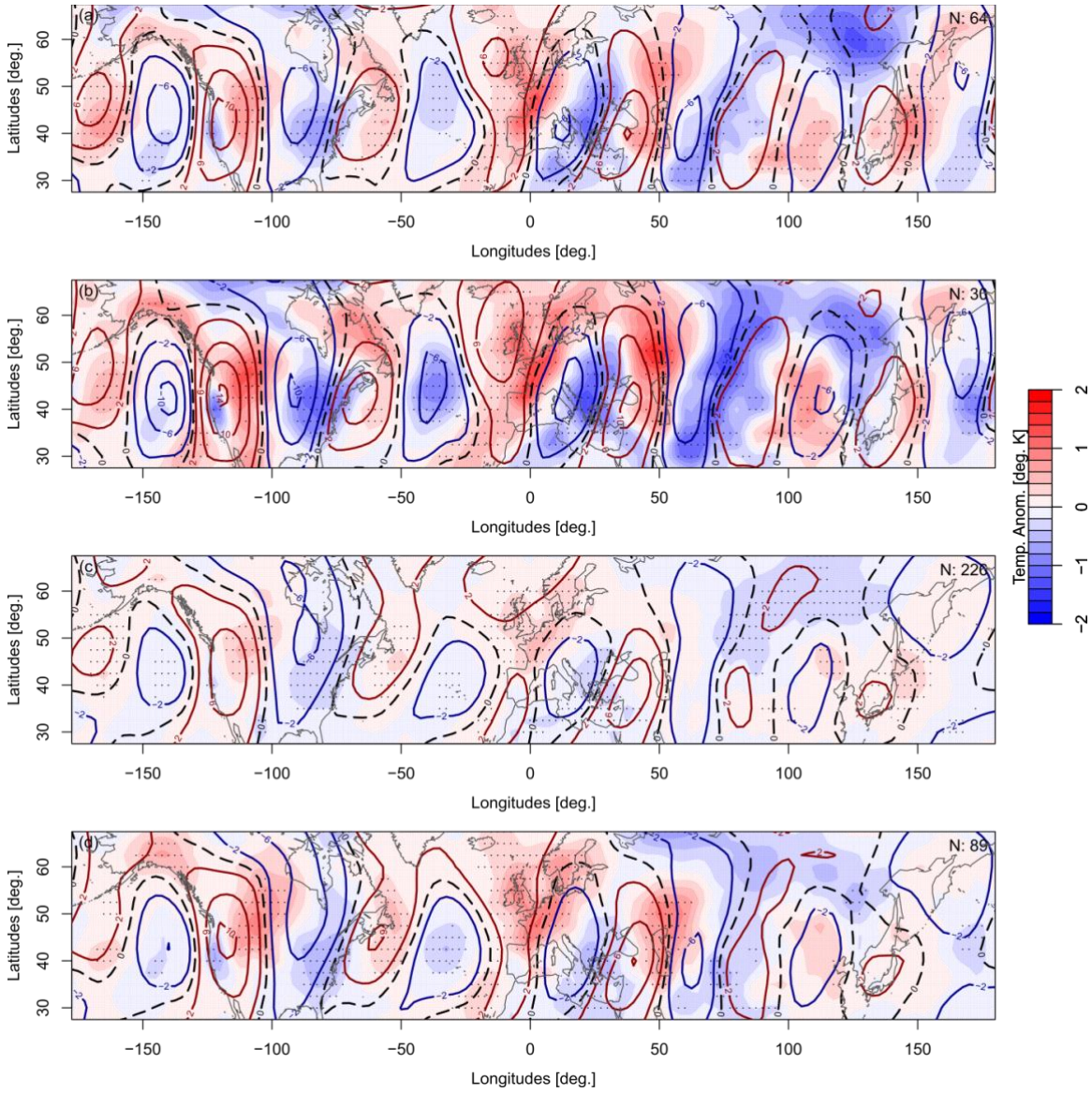

Figure S5. The recurrent wave-7 teleconnection. Composite temperature anomalies (filled contours) and meridional wind velocities (southward: red line contour, northward: blue line contour, zero wind line: black line) during weeks of wave-7 amplitude in summer (JJA, 1979 – 2016) **(a)** within the preferred phase position (see Fig.S3a, phase locked from here on) and above average, **(b)** phase locked and above 1σ, **(c)** above average irrespective of phase position, **(d)** above 1σ irrespective of phase position. Continental coastlines are depicted by grey outlines. The respective number N of averaged weeks is given in the upper right corner. Grey dots mark the grid-points where anomalies are significantly different (95% confidence level) from the remaining weeks. Note that unlike in Fig. 3a,b shown in the manuscript no false discovery rate significance testing (FDR(2)) was applied here.

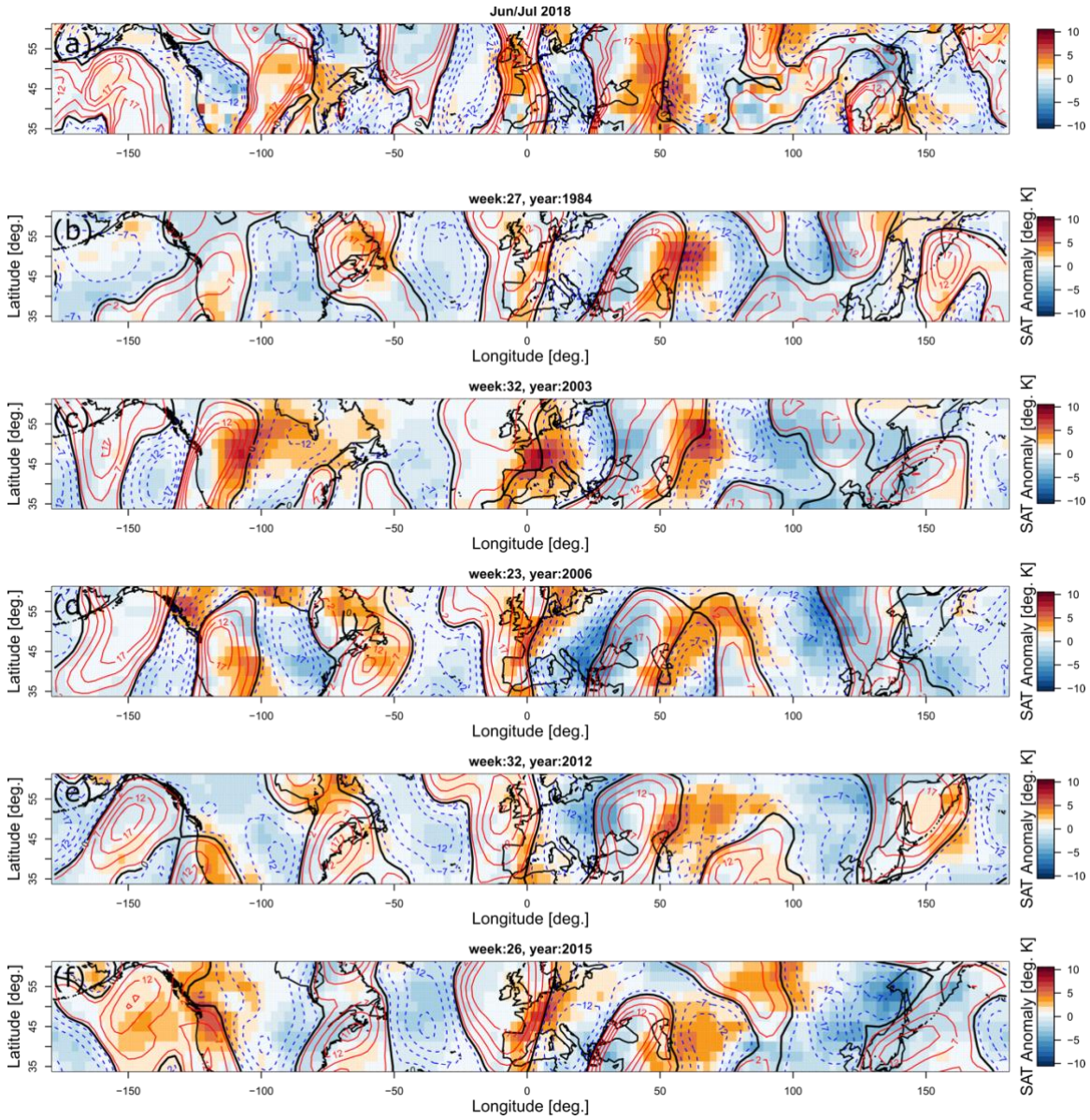

Figure S6. Hemispheric temperature and circulation extremes over the recent past. (a) Surface temperature anomalies (compared to 1981-2010 climatology, filled contours) and meridional winds (line contours, North-South: blue, South-North: red) in a 15-day running-mean centered around 1 July. **(b–f)** Same variables shown during selected examples of this pattern observed during summers of severe heatwaves in the Northern Hemisphere based on weekly means, including the severe European heatwaves of **(c)** 2003 and **(f)** 2015. For a full list see table S1.

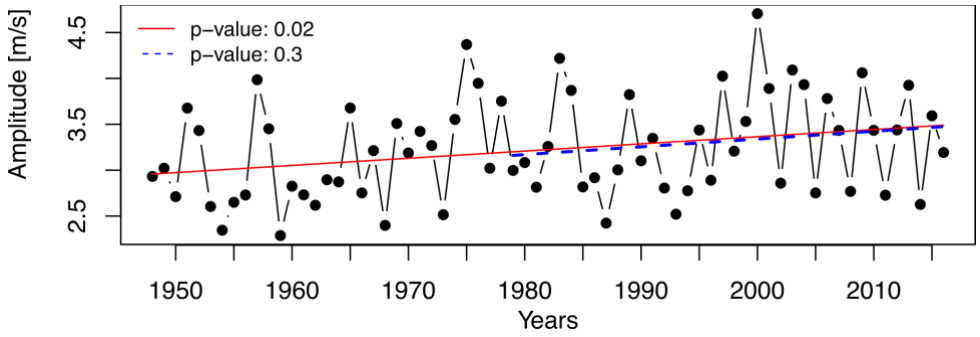

Figure S7. Long term trends in wave 7 amplitude. Mean wave 7 amplitude in summer (June-August) from over the period 1948 – 2016. Linear trends for the entire period (red solid line) statistically significant but might be spurious due to changes in measurement systems. Trends over the satellite-based measurement period (1979-2016) increasing but are not significant.

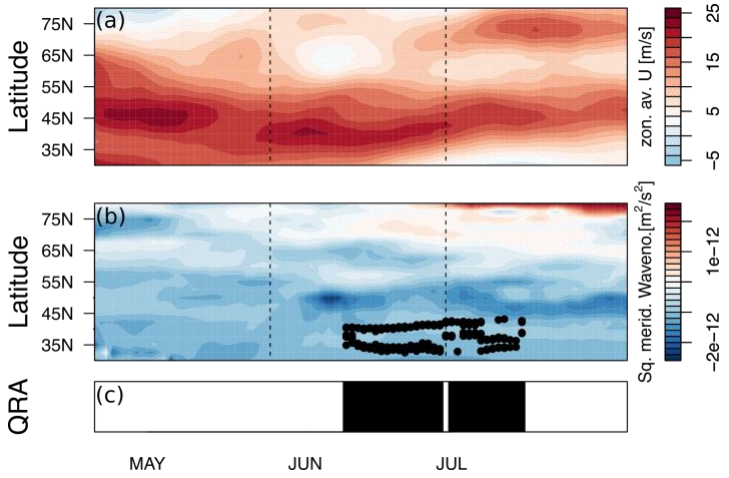

Figure S8. Resonance detection of wavenumber 7 early Summer 2018. (a) Time-series of zonally averaged zonal wind. A 'double jet pattern' forms at the beginning of June in the zonal mean. **(b)** Squared meridional wavenumber. A waveguide, the key condition for wave resonance, forms in the mid-July for wavenumber 7, as shown by the black dots. **(c)** Resonance is detected from mid-July on (marked in black).

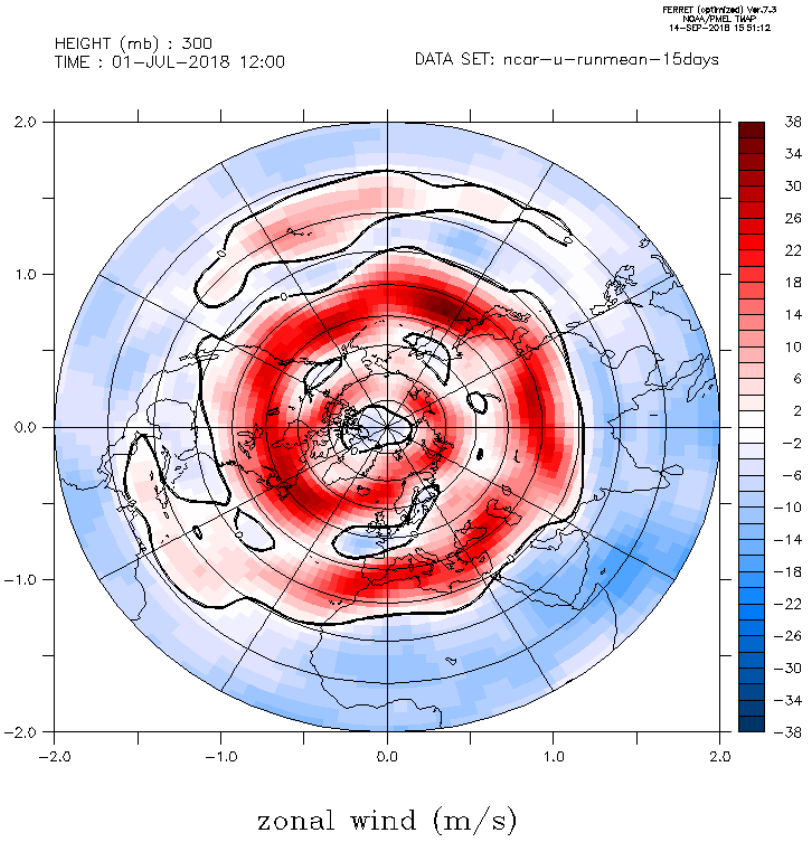

Figure S9. Zonal wind component in the upper troposphere. Shown is the 15-day mean, centered on July 1st 2018. A strong subtropical jet is visible over the entire longitudinal belt which splits into a double jet pattern over the Eurasian continent at about 15°W. The jet shows positive values around the entire hemisphere, thus providing a waveguide which can be considered circumglobal.

Year	Month	First day of week
1979	6	29
1980	6	1
1983	7	6
1983	7	13
1984	6	15
1985	6	29
1988	6	29
1989	6	15
1989	7	13
1989	7	27
1991	8	17
1995	7	6
1996	7	13
1997	6	1
1997	8	24
1998	8	3
2000	6	29
2000	7	20
2001	6	22
2003	7	6
2003	7	13
2003	8	3
2003	8	10
2004	7	13
2005	6	15
2006	6	1
2006	6	8
2009	6	1
2009	6	22
2009	6	29
2010	6	8
2010	6	29
2010	7	6
2012	6	22
2012	8	10
2013	6	22
2013	6	29
2015	6	29
2015	8	10
2015	8	24

Table S1. Dates of weeks with wave number 7 above 1.5σ, as used in the analysis shown in Fig. 3 a, b.

i. *Waveguide for synoptic scale free wave k:*
1. Two turning points (TPs, change of sign) in l^2
2. $l^2 > 0$ between the turning points (TP)
3. $U > 0$ in between and in the vicinity of the TPs
4. The highest value of l^2 between the TPs is in the range of l^2_{min} and l^2_{max}
5. The TPs lie within a region of 30°N and 70°N
6. The TPs have a minimum distance of w_k
7. In case of two waveguides their distance has to exceed at least 5°
ii. *Effective Forcing Amplitude for forced planetary wave $m \approx k$:*
8. The effective forcing Amplitude A_{eff} for a respective wave number m has to exceed a certain threshold q_k, defined by the 50th percentile of the overall wave spectrum on a specific timestep.

Table S2. Key Conditions for resonance detection from (10)

References:

1. Kalnay, The NCEP/NCAR 40-year reanalysis project. Bull. Am. Meteorol. Soc., 437–470 (1996).

2. D. Wilks, " the Stippling Shows Statistically Significant Grid Points ." Bull. Am. Meteorol. Soc. 97, 2263–2274 (2016).

3. D. Coumou, V. Petoukhov, S. Rahmstorf, S. Petri, H. J. Schellnhuber, Quasi-resonant circulation regimes and hemispheric synchronization of extreme weather in boreal summer. Proc. Natl. Acad. Sci. 111, 12331–12336 (2014).

4. V. Petoukhov, S. Rahmstorf, S. Petri, H. J. Schellnhuber, Quasiresonant amplification of planetary waves and recent Northern Hemisphere weather extremes. Proc. Natl. Acad. Sci. 110, 5336–41 (2013).

5. V. Petoukhov et al., Role of quasiresonant planetary wave dynamics in recent boreal spring-

177 to-autumn extreme events. Proc. Natl. Acad. Sci. 113, 6862–6867 (2016).

178 6. K. Kornhuber et al., Summertime Planetary Wave-Resonance in the Northern and Southern
179 Hemisphere. J. Clim. 30, 6133–6150 (2017).

180 7. B. J. Hoskins, D. J. Karoly, The Steady Linear Response of a Spherical Atmosphere to Thermal
181 and Orographic Forcing. J. Atmos. Sci. 38, 1179–1196 (1981).

182 8. G. Branstator, H. Teng, Tropospheric Waveguide Teleconnections and Their Seasonality. J.
183 Atmos. Sci. 74, 1513–1532 (2017).

184 9. G. Branstator, Circumglobal Teleconnections, the Jet Stream Waveguide, and the North
185 Atlantic Oscillation. J. Clim. 15, 1893–1910 (2002).

186 10. K. Kornhuber, V. Petoukhov, S. Petri, S. Rahmstorf, D. Coumou, Evidence for wave resonance
187 as a key mechanism for generating high-amplitude quasi-stationary waves in boreal summer.
188 Clim. Dyn. 49, 1961–1979 (2017).

189 11. L. Stadtherr, D. Coumou, V. Petoukhov, S. Petri, S. Rahmstorf, Record Balkan floods of 2014
190 linked to planetary wave resonance. Sci. Adv. 2, e1501428 (2016).

191 12. V. Petoukhov et al., The role of quasi-resonant planetary wave dynamics in recent boreal
192 spring-to-autumn extreme events. Proc. Natl. Acad. Sci. 113, 6862–6867 (2016).

193 13. I. M. Held, (Academic Press, London, 1983), pp. 127–168.

194 14. I. Manola, F. Selten, H. De Vries, W. Hazeleger, “Waveguidability” of idealized jets. J.
195 Geophys. Res. Atmos. 118, 10432–10440 (2013)

196